Optica Applicata, Vol. LII, No. 3, 2022
DOI: 10.37190/oa220311

Spatial light modulator design and generation of structured electromagnetic waves using digital light processors

F. YALCINKAYA[1], T. KOC[1, 2*], Z. PALA[3]

[1]Kirikkale University, Department of Electrical and Electronics Engineering, Kirikkale, Turkey

[2]Bitlis Eren University, Department of Electrical and Electronics Engineering, Bitlis, Turkey

[3]Mus Alparslan University, Department of Computer Engineering, Mus, Turkey

[*]Corresponding author: trkkc88@gmail.com

Spatial light modulators (SLMs) are versatile devices used for optical studies. These instruments have a wide area of application in photonics. Additionally, SLMs have potential utility in different applications, such as biomedical applications, laser based surgery for precise cutting and as optical tweezers to separate cells in a petri container. However, the high cost of SLM devices prevents their widespread use in many areas, including industrial areas and scientific research laboratories. This paper demonstrates how to design a digital light processor (DLP) based low-cost SLM and describes how to obtain structured electromagnetic waves with the designed SLM. Therefore, this research was undertaken to design and produce a low-cost SLM device for optical applications. For this purpose, two prerequisites had to be fulfilled, the first was to use suitable components of a projection device with DLP-based digital micro-mirror device (DMD), and the second was to eliminate unnecessary SLM components from the system. Finally, holographic images reflected on the SLM screen were created by using Mathematica software program to change the amplitude and phase of the electromagnetic waves in order to obtain the structured electromagnetic waves.

Keywords: spatial light modulator, digital micro-mirror device, digital light processing, structured electromagnetic waves, orbital angular momentum, hologram.

1. Introduction

For electromagnetic waves, wavelength, frequency, and amplitude are the most basic three parameters. The release of electromagnetic waves (EMW) from the source at certain intervals demonstrates a time-dependent distribution. These waves can also be spatially structured in case they pass through a dielectrically inhomogeneous environment while travelling through space. By utilization of this function, DLPs are playing an important technological role by enabling the generation of spatially-structured EMWs.

Structured EMWs are examined in two different forms, twisted lights and orbital angular momentum (OAM). These waves have been a subject of interest for many scientific fields, such as quantum mechanics, nanophysics, optics, materials science, optoelectronics and communications; thus, a great number of studies have been focused on structured EMWs [1–4]. When these studies are closely examined, it is easy to see that SLMs play an important role for the generation of spatially-structured EMWs.

The SLM is an optoelectronic tool that modulates the amplitude and phase of EMWs, and SLM devices are widely used in various research areas, such as fiber optic communication [1, 5], ultrafast pulse shaping [2], microscopic laser surgery [3], optical information processing, programmable imaging, electrostatic printing [4], and imaging applications [6]. More specifically, it is possible to observe SLM use in many areas that require manipulation of the spatial profile of light beams [7–11]. For example, by using SLMs, it is possible to dynamically illustrate diffraction, interference, and holography concepts with real-time control over model parameters. Thus, SLMs make it possible to perform new experiments that cannot be conducted with standard laboratory equipment. For these reasons, making SLMs available in optical laboratories, where academic and scientific studies are carried out, will be a useful contribution for researchers studying diffraction, Fourier optics, image processing and signal processing techniques.

SLMs have two different display types: DMD and liquid crystal display (LCD). Developed by Texas Instruments, DLP-based DMDs can be used as SLMs and also as micro-electro-mechanical systems (MEMS). The DMD is made of thousands of moving micro-mirrors in number which are controlled via CMOS technology. Moving micro -mirrors are highly reflective and that characteristic can efficiently be used to modulate light. Therefore, as an optical, highly reflective and efficient MEMS, DMD can be referred to as both a reflective SLM [8] and a widely used display chip for holographic displays [6, 12–14].

On the other hand, LCDs which are highly reflective, can be used to modulate light, and are a popular option for holographic displays, indicating some similarities with DMDs. The resolution, display panel ratios, and pixel size of DMD for holographic displays are not much different from LCD display chips. In addition to these similar features with DMDs, they also have some superiorities compared to other screen chips. These are high resolution and very high-velocity response, as well as their capability in providing deep separation between the generated image, reconstructed beam, and the binary hologram display.

The DMD feature using its very high-speed response can allow the presentation of colors and gray levels, so as to increase both the resolution and size of the reconstructed image by time multiplexing technique [12, 13]. It can be asserted that DMD is a very handy tool for applications ranging from 3D computational imaging [15] to neuronal activity control in optogenetics [16], due to its high-velocity response, wide operating spectral band range, and high power threshold. In recent studies, DMDs have been used to encode a variable phase structure onto a beam [17, 18].

Because of the aforementioned features, it may be possible to design and construct a lower cost SLM by using a projection device with a DMD screen. In this study, first of all, a DLP-based low-cost SLM was designed using parts taken from second-hand equipment. In order to obtain structured electromagnetic waves, holograms were created by the Mathematica software program. These holograms were loaded on the DMD and then structured electromagnetic waves were obtained as a result of the reflection of the laser beam sent onto the DMD.

2. Computer-generated hologram

Computer-generated holography (CGH) deals with the methods used to produce digital holograms. The hologram can then be printed onto a film or loaded into an SLM for holographic reconstruction. CGHs have the advantages that three-dimensional objects do not have to exist in the real world. In other words, the objects may be imaginary but not real. For the generation of CGHs, different computational methods have been developed for various imaging devices and reconstruction methods.

Usually CGH is a binary representation of a two-dimensional (2D) Fourier transform of a specific image. To reproduce or reconstruct the image from the hologram at a later stage requires the use of a lens working on Fourier transform principles. Recently, there have been a lot of publications about CGH, as an active area of research. For example, CHUYING YU *et al*. [19] explored quaternion Fresnel transform, chaos and encryption scheme based on CGH. A hologram calculation method has been developed by SCHWERDTNER [20] to reconstruct a holographically created object using an imaging device. LEISTER *et al*. [21] developed a new method helping to obtain a suitably coded hologram with which an observer looking through the observer's window could reconstruct an observed three-dimensional (3D) scene. Besides these studies, one group of the most commonly used hologram types of CGH is called detour-phase-type holograms and there are a lot of research using that hologram types [22–24]. For example, BROWN and LOHMANN [25] reconstructed the hologram by choosing a phase different from the Fourier transform phase. TRIPATHY *et al*. [26] proposed an algorithm based holographic grating design in order to obtain the desired diffraction efficiency [27].

2.1. Lohmann's hologram

The emergence of modern digital holography can generally be said to begin with the work of LOHMANN *et al*. in the mid-sixties [28]. A Lohmann hologram (or the detour -phase hologram) is a sampled Fourier transform of a specific image. The Fourier transform properties of a positive lens are used for the reconstruction of the image in a Fourier Transform hologram. So this process consists of two steps: Performing a sampled Fourier transform of a specific image and then using a Fourier transform lens to reconstruct the desired image from the hologram (Fig. 1). Fourier-based CGH can only reconstruct 2D images. BROWN and LOHMANN [25] developed a technique to reconstruct the CGH of 3D objects. Calculation of light emitted from 3D objects is performed ac-

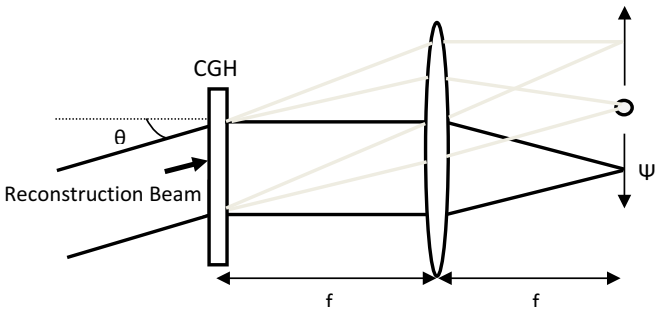

Fig. 1. Reconstruction scheme for the Lohmann hologram [27].

cording to the usual parabolic approach to the Fresnel–Kirchhoff diffraction integral. Therefore, the waveform to be constructed by the CGH is the superposition of the Fourier transform of each object plane at depth modified by a quadratic phase factor.

An optical scheme has been developed for the reconstruction of a Fourier hologram according to the Lohmann method shown in Fig. 1. The Lohmann method divides the hologram plane into smaller rectangles such as each rectangle contains an aperture [28]. Figure 2 shows the structure of a Lohmann cell. The amplitude is controlled by the

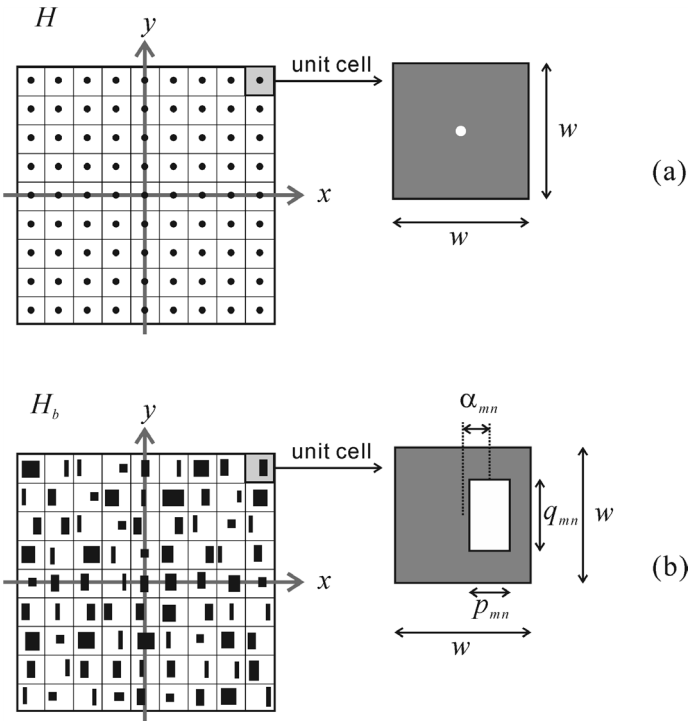

Fig. 2. Cell definition (**a**) a complex hologram and (**b**) a detour-phase binary hologram [29].

size of the aperture. The adjustment of the phase determines the position of the aperture, which results in the binary transfer model.

Figure 1 shows the setup for the Fourier hologram reconstruction via Fourier transform lens with a focal length of f. The relationship between the $H(x, y)$ hologram and the amplitude of the reconstructed image $[\Psi(x, y)]$ is given by the following equation:

$$\Psi(x, y) = \mathcal{F}\{H(x, y)\Psi_{\mathrm{r}}(x, y)\}_{k_x = k_0 x/f,\ k_y = k_0 y/f} \tag{1}$$

Here $\Psi_{\mathrm{r}}(x, y) = \exp(-jk_0 \sin\theta_x)$ shows the amplitude of a plane wave reconstruction light in complex mathematical form, where θ is the angle of inclination.

In general, the hologram is a complex mathematical function of the form, $H(x, y) = a(x, y)\exp[-j\varphi(x, y)]$, where $a(x, y)$ and $\varphi(x, y)$ are the amplitude and phase of the hologram, respectively. Therefore, our goal is to design the binary amplitude model $H_{\mathrm{b}}(x, y)$ function, which is similar to the complex function $H(x, y)$ hologram. If it is limited to a $m \times n$ window in the reconstruction plane, then it is possible to find $H_{\mathrm{b}}(x, y)$ to be inside the window:

$$\mathcal{F}\{H_{\mathrm{b}}(x, y)\Psi_{\mathrm{r}}(x, y)\} \approx \mathcal{F}\{H(x, y)\Psi_{\mathrm{r}}(x, y)\} \tag{2}$$

First, the area of hologram consists of a number of unit cells, and the size of each cell is defined as $w \times w$, as shown in Fig. 2. In case of the complex hologram $[H(x, y)]$, both $a(x, y)$ and $\varphi(x, y)$ are assumed to have slow change within any given cell. The cells can then be replaced with a series of point sources, resulting in a complex hologram sampled as follows:

$$H_{\mathrm{s}}(x, y) = \sum_{m \times n} a_{mn}\exp(-j\varphi_{mn})\delta_{mn}(x - x_m, y - y_n) \tag{3}$$

where (m, n) $x_m = mw$, $y_n = nw$; $a_{mn} = a(x_m, y_n)$ and $\varphi_{mn} = \varphi(x_m, y_n)$ are the indices of the centered cell.

A sampled complex hologram $H_{\mathrm{s}}(x, y)$ can be simulated by using the binary hologram by opening of a transparent aperture on an opaque background of an area proportional to a_{mn}. The phase of the light is controlled by a slight shift of the aperture center. The opening in each cell is a rectangular shape of size $p_{mn} \times q_{mn}$. Thus, the binary hologram can be expressed as [29]:

$$H_{\mathrm{b}}(x, y) = \sum_{m \times n} \mathrm{rect}\left(\frac{x - x_m - a_{mn}}{p_{mn}}, \frac{y - y_n}{q_{mn}}\right) \tag{4}$$

3. Materials and methods

DMDs are designed to modulate light robustly. Modulation structures are based on switching, as in sigma-delta modulation, and give satisfactory results in imaging. If

DMDs are compared with the latest developments in LCDs, it can easily be determined that DMD technology has a high switching speed (~30 μs) with respect to LCDs [30, 31]. However, refraction elements in LCDs have a lower switching speed (~20 ms). DMD technology offers better performance in terms of both optical fill-factor and light transmission than LCD technology. These parameters have values 94% and 98 in DMDs, while LCDs have corresponding values of 93% and 90%, respectively. However, the pixel size of LCD technology (3.74 μm) is better than the pixel size of DMD (5.4 μm). The recent technological developments in switching speed, optical fill factor and light transmission and pixel size in DMD and LCD technologies allow SLMs to be used at wavelengths between 355 and 400 nm [17, 18].

In this study, the comparison of a DMD-based SLM with a commercial LCD-based SLM, in terms of cost and features, is shown in Table 1. In addition, it must be noted that the method used to convert the projector into an SLM can also be applied to any other projector or projection device.

The lower-cost SLM is designed by using the parts taken from a second hand DLP-based projector. The size of the pixel array of the DMD in this projector was 1024 × 768 pixels. Pixel size, diffraction efficiency, and inter-pixel clearance information of the DMD were 10.8 μm, 86%, and 1 μm, respectively. The effective reflection rate for visible light was approximately 88%. Each micromirror in the DMD could be adjusted to be tilted at +12 0 –12 degrees.

T a b l e 1. DMD panel specifications of the projector converted to SLM [34].

DMD Parameters	Description
The family of chipset	DLP5500
The component type	DMD
The wavelength of the ilumination (min) (nm)	420
The wavelength of the ilumination (max) (nm)	700
The array size of the micromirror	1024 × 768
The binary pattern rate (max) Hz	5000
The pixel data rate (max) (Gbps)	3.9
The pitch of micromirror (μm)	10.8
The resolution of display (max)	1024 × 768 (XGA)
The pattern rate, 8-bit (max) (Hz)	500
Micromirror array orientation	Orthogonal
The tilt angle of the micromirror (relative to flat state)	±12°
The size of the screen	0.55-inch micromirror array diagonal
The window transmission	97% (single pass, through two window surfaces)
The reflectivity of the micromirror	88%
The efficiency of the array diffraction	86%
The fill-factor of the array fill	92%

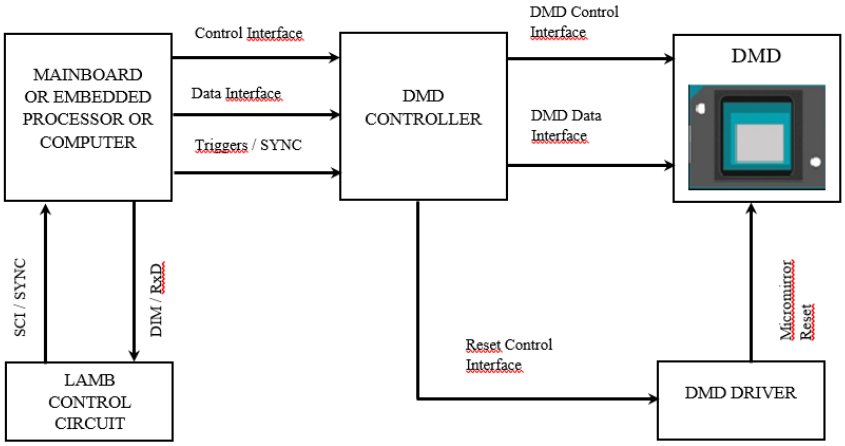

Fig. 3. DLP-based spatial light modulator block diagram.

The SLM was created by modifying the BENQ MX511 DLP projector, which was a second-hand purchase for $17.57. This projector uses a DLP5500-DMD panel to modulate the light. The DMD panel used is a high resolution DMD because it has more than 750000 micro mirrors, and the SLM obtained modulates the amplitude, direction and/or phase of the incident light. This DMD can modulate electromagnetic waves between 420 and 700 nm wavelength. DMD properties are given in Table 1.

The cooling fan of the DLP projector was transferred into the SLM, using the control circuit, mainboard, and DMD display. The block diagram of the converted DLP-based SLM device is given in Fig. 3.

The lamp of the projector device was deactivated by a special method, as it was unnecessary for the intended design. In order to better understand the deactivation of the lamp, it is useful to explain the operational management of the lamp. Briefly, according to the standard universal asynchronous receiver-transmitter (UART) protocol application note of OSRAM, the serial communication interface (SCI) signal has a higher opening priority than the UART software command [35]. A signal goes from the mainboard to the lamp control circuit for the projector to work via PN5, as seen in Table 2, and the device starts to operate when a signal comes from the control circuit to the mainboard via PN4.

T a b l e 2. Lamp control circuit pin diagram.

Pin No.	Pim diagram
PN1 (Pin Number 1)	Phototransistor Collector - Flag / TxD+
PN2 (Pin Number 2)	Phototransistor Emitter - Flag / TxD-
PN3 (Pin Number 3)	LED Anodes - Common LED+
PN4 (Pin Number 4)	Cathode LED - SCI / Sync.
PN5 (Pin Number 5)	Cathode LED - DIM / RxD

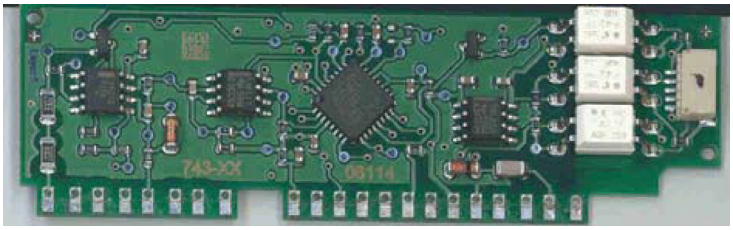

Fig. 4. The lamp control circuit [35].

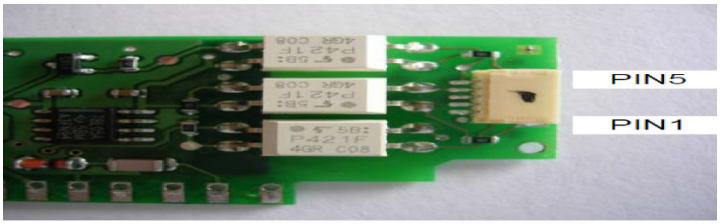

Fig. 5. Lamp control circuit pin assignment [35].

PN1 and PN2 data lines in Table 2 include the mainboard electronic output of the device, and PN5, as a data line, has an input line to derive the lamp. All interface lines, optically isolated from the grid, utilizes the three opto-couplers to provide extra-low voltage security isolation. The interface of the lamp control circuit has to drive the LED lines (PN4 and PN5) with nominal current, and detect the phototransistor output state (PN1 and PN2) and convert it into a suitable digital signal. The data lines used to cancel the lamp out on the projector are PN4 and PN5.

The method used for the cancellation of the lamp control circuit and pin diagram is as follows: As shown in the pin diagram in Table 2, PN5 and PN4 lines are data pins that control whether the lamp between the lamp control circuit and the mainboard is working. When the lamp is removed from the projector, the data communication between the mainboard and the lamp control circuit is necessary for the device to function properly. Therefore, a button is installed between PN4 and PN5 shown in Figs. 4 and 5. After pressing the power button of the SLM device and by pressing the button installed between PN4 and PN5, data communication will be provided between the mainboard and the lamp control circuit.

Like the lamp in the projector, lenses are also unnecessary for the SLM. Since the separation of the lenses and metal parts in front of the DMD in the device is a purely mechanical process, these parts were easily removed from the system.

After all these processes, the SLM is ready to work. Figure 6 shows the DLP-based projection device converted to SLM. The parts numbered 1, 2, and 3 are the button attached to cancel the lamp control circuit, the DMD, and the mainboard, respectively.

The SLM device, designed with a new approach, was compared with similar products, including one commercial product. Comparisons with Model LC2012 (Holoeye) and two other DLP-based SLMs are given in prior literature [36, 37]. As shown by

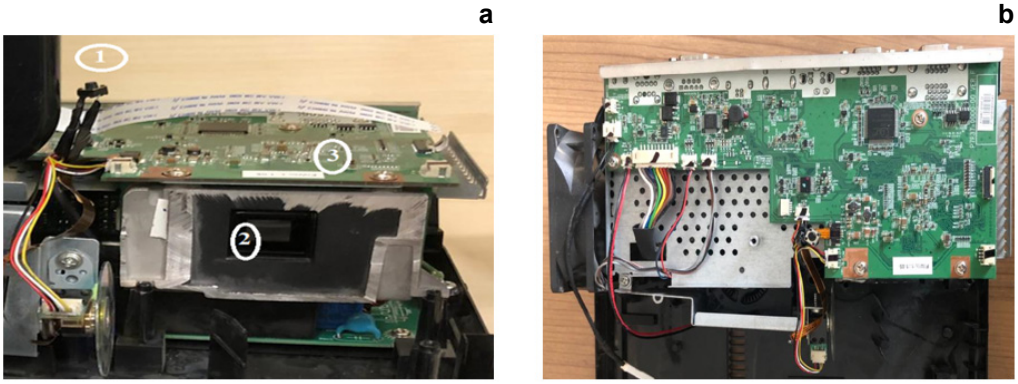

Fig. 6. DLP based spatial light modulator: (**a**) modulator components and (**b**) top view of the main board.

T a b l e 3. Comparison of the SLM device we designed with other SLM devices.

Features	SLM (this paper)	DLP4710-DLP evaluation module [36]	DLP2000-DLP evaluation module [37]	LC2012 SLM
Screen type	DMD	DMD	DMD	LCD
Resolution	1024 × 768 pixel	1920 × 1080	640 × 360	1024 × 768 pixel
Pixel pitch	10.8 µm	5.4 µm	7.6 µm	36.0 µm
Input frequency	60 Hz	120 Hz	120 Hz	60 Hz
Signal format	HDMI	HDMI	HDMI	HDMI
Product price	17.57$	~1500$	~200$	~ 4672$

Table 3, the SLM we converted from the projector was obtained at a very low cost when compared with available counterparts. The basis of the SLM design, which is the subject of this paper, is a used DLP-based second-hand projector device purchased only for 17.57 US dollars.

4. Holographic mask design and electromagnetic waves with angular momentum

Electromagnetic waves with angular momentum appear as a central dark ring of light when viewed from a vertical plane along the axis [38]. The phase of a light beam is bendable around its propagation axis like a corkscrew. When the light wave is expressed by a complex number in the form $X.\exp(i\beta)$, the ratio of the azimuthal angle of the cylindrical coordinate plane (r, φ, z) to the phase distribution is defined as "curling", where X is the amplitude of the field and β is the phase of the wave front. On the other hand; r, φ, and z parameters express radial distance, polar angle, and azimuth angle, respectively. Due to the curl, the light wave disappears along the z-axis. If the value φ of the angular coordinate system is not well-defined at $r = 0$, that leads to a phase single uniqueness where the amplitude disappears [7, 38]. $\beta = m\varphi$ is defined by a helical phase

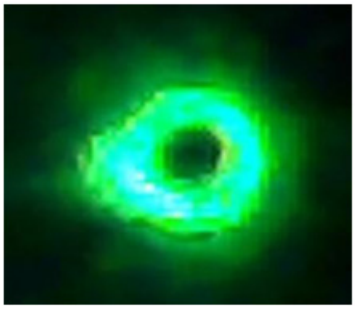

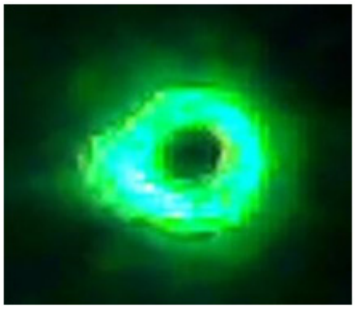

Fig. 7. Two beams with the same load running in a parallel direction: (**a**) image moves in a counterclockwise rotation (**b**) image moves clockwise.

distribution. Such a beam of light looks as a bright ring with a dark hole at the center on a flat surface as shown in Fig. 7. To ensure the continuity of the field, the integer value of m at $\varphi = 2\pi$ indicates the number of phase windings around the dark spot.

The topological charge of the vortex, called m, is a number. Physically it is the phase rotation velocity around the singularity; it takes two values either positive or negative, in other words counterclockwise rotation or clockwise rotation, respectively, means [38]. The parameter m is defined by the z-component of angular momentum L_z. The L_z value per photon for the light beam is obtained by dividing the Planck's constant ($\hbar$) by 2π.

$$L_z = -i\hbar \frac{\partial \beta}{\partial \varphi} = -i\hbar m \tag{5}$$

The continuity condition at $\varphi = 2\pi$ implies the quantification of the angular momentum. The value of the L_z parameter indicates that, as the beam progresses, the momentum vector **p** becomes a rotation around the black hole.

Electromagnetic waves with angular momentum can be generated by manipulation of the laser cavity [38, 39], using mod converters [40], or a simple technique using computer-generated holograms [41, 42]. Generating holograms by computer is a simple technique [42]. Many studies have shown how to design computer-generated holograms [43, 44]. Our aim is to obtain the H hologram transmission function by placing the $\exp(im\varphi)$ phase into a Gaussian beam and interference of the reference inclined plane wave of $\psi_1 = \exp(ikx)$ and the object wave of $\psi_2 = \exp(im\varphi)$ carrying the singular phase. Here k is a spatial frequency showing the tilt angle of the wave. When a beam of light with a reference wave is struck into this hologram, the output beam will be reconstructed to appear as a beam with angular momentum. Equation (6) shows the H hologram transmission function. The holographic mask design, consisting of light and dark lines, was obtained by using the H hologram transmission function in Eq. (6) with the Mathematica software.

$$H = \left|\psi_1 + \psi_2\right|^2 = \left|\exp(ikx) + \exp(im\varphi)\right|^2 = 2\left[1 + \cos(kx - m\varphi)\right] \tag{6}$$

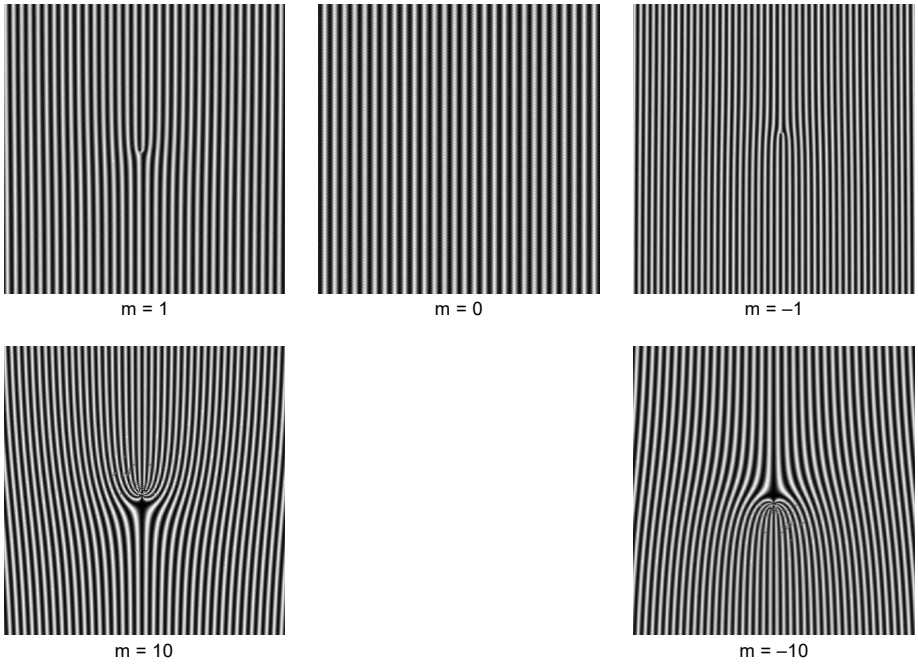

Fig. 8. Different drawings of $H = |\psi_1 + \psi_2|^2$ are shown for different m topological values using Eq. (2).

Here $\tan(\varphi) = (y/x)$ is the polar coordinate. Hologram masks with different m topological values are shown in Fig. 8.

In case, one of holographic patterns is illuminated by a w-wide Gaussian beam, $\psi_G = \exp(-r^2/w^2)$, then the resulting pattern is the far-field Fraunhofer diffraction pattern. Far-field Fraunhofer diffraction pattern is proportional to both the Fourier transform of the input function ($\psi_G H$) and H hologram transmission function [38]. Thus, the brightness on the remote surface with the help of computer generation is obtained by the following equation:

$$I = \mathrm{F}[\psi_G H] = \mathrm{F}\left[\exp\left(-\frac{r^2}{w^2}\right)\left|\exp(ik_x x) + \exp(im\varphi)\right|^2\right] \tag{7}$$

Here k_x is the x-component of the wave vector of the oblique wave. As a result, it can be calculated and drawn with a standard math software program. Gaussian rays with topological values of the Fourier transform of $\psi_G H$ $m = 5$ and $m = -5$ are shown in Fig. 7.

The light intensity is the same for the two vortices shown in Fig. 7. However, phase spreads turn in opposite directions. In other words, if rotation is counterclockwise for $m = 5$, then it is $m = -5$ for clockwise rotation. As a result, a complete reconstruction of the ψ_2 object beam (in azimuth phase) is obtained when the hologram mask is illuminated with a laser beam identical to the reference wave beam ψ_1 used to record the

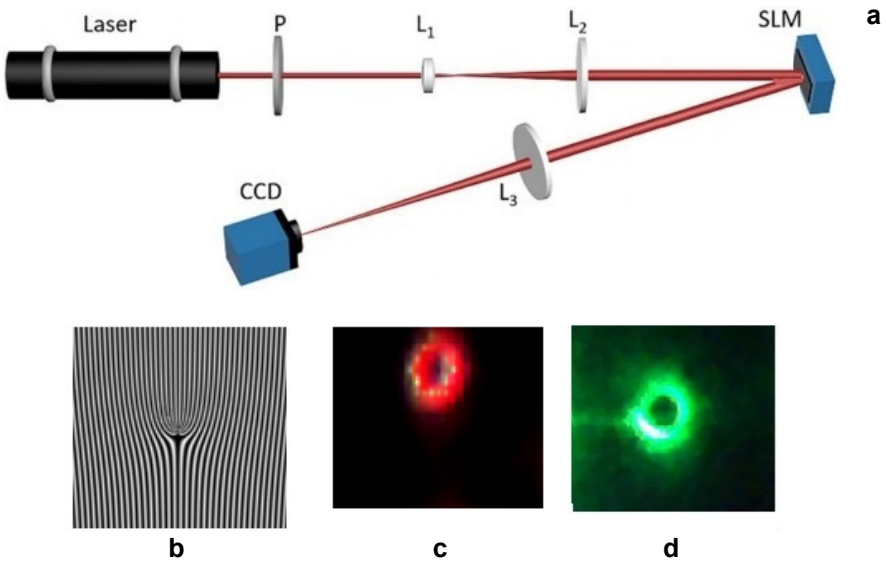

Fig. 9. (**a**) Experimental setup for structured EMW generation and detection. In the experimental setup; P – polarizer, L – lens, SLM – spatial light modulator, CCD-CCD camera. (**b**) CGH hologram uploaded to SLM. (**c**) Angular momentum value $m = -5$ structured EMW. (**d**) Angular momentum value $m = +10$ structured EMW.

hologram [41]. Hologram mask patterns corresponding to the topological value of m are shown in Fig. 8.

The experimental setup schematic for obtaining a structured EMW with a device converted to a second-hand SLM is shown in Fig. 9. The beam sources used in the production of structured EMW are given in Fig. 9**c** with 13 mW laser operating at 640 nm and in Fig. 9**d** with 100 mW laser operating at 532 nm. P polarizer was used to select vertical polarization. P beam containing the EMW, L_1 and L_2 passes through the expanders, then illuminates a CGH-generated hologram with controllable pixels loaded into an SLM. Different holograms are used to create structured EMWs with different topological values. The CGH seen in Fig. 9**b** has been loaded into the SLM. Structured EMW is formed by reflection and diffraction. As shown in Figs. 9**c** and 9**d**, the structured EMW with topological value of $m = -5$ and $m = +10$ is obtained, respectively. The far-field diffraction pattern is captured by a CCD camera in the Fourier plane of the convex lens (L_3).

5. Results and discussion

The hologram mask created with the Mathematica software program was uploaded to the DMD, and the laser light was dropped on the hologram on the DMD. Ultimately, the structured EMW was obtained by reflecting the laser light back over the DMD mirror. In this study, it has been shown that the device designed can be used as an SLM. At the same time, it has been shown that the designed device can be produced at a much

lower cost than existing SLMs. There are similar studies when the literature on the subject is examined, however, Table 3 shows that SLM we designed has a lower cost compared to other studies [36, 37], and in this respect, a contribution to the literature.

Structured EMWs were obtained by establishing a basic experimental setup with SLM, and said structured EMWs were recorded with CCD (charge coupled device).

DMD illumination wavelengths in the modified SLM range are from 420 to 700 nm. Laser beams with different wavelengths, 640 nm red and 532 nm green, are used to show that the modified SLM works within the range of wavelengths. The results obtained demonstrate the correct and proper working conditions of the modified SLM system.

The records of the CCD images of the structured red (620–700 nm) and green (500 –570 nm) laser light obtained with the DLP based SLM are shown in Fig. 10. Figure 11 shows structured electromagnetic waves falling on a flat surface. Figure 11 shows the structured EMW pairs with absolutely the same topological load values. For better understanding of Fig. 11, one structured EMW pair with absolutely the same topological charge value is considered in Fig. 12.

The topological charge value of the red laser beams at 620–700 nm is m = ±10 as shown in Fig. 12**a**. The topological load value $m = -10$ rotates clockwise while $m = +10$ rotates counterclockwise. The topological charge value of the green laser beam

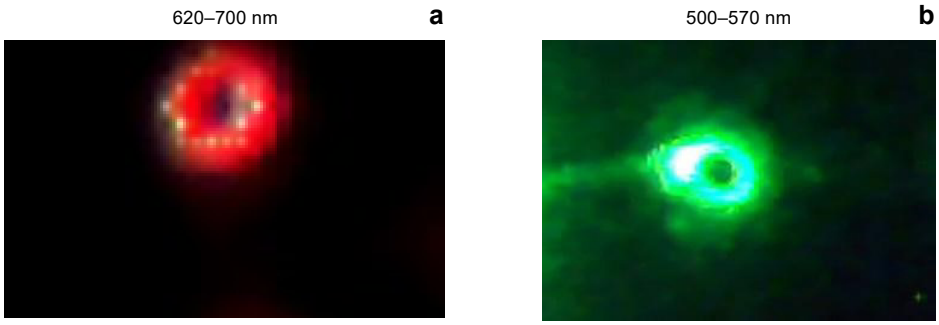

Fig. 10. Structured electromagnetic waves recorded with a CCD camera. (**a**) Topological values in red (620–700 nm) laser sequence for $m = -5$. (**b**) Topological values in green (500–570 nm) laser sequence $m = -5$.

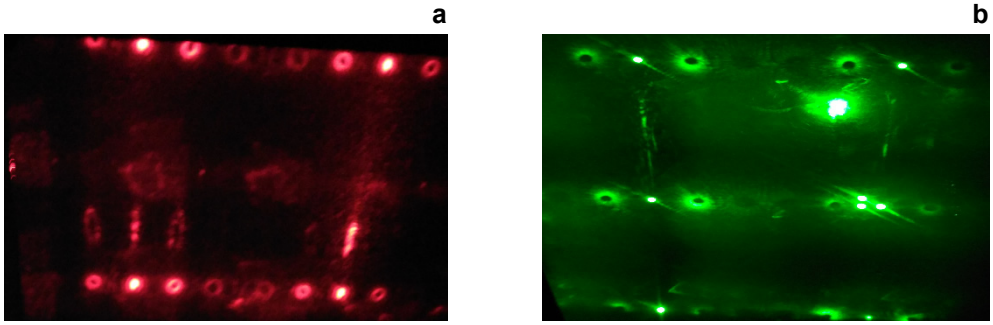

Fig. 11. Structured electromagnetic waves. (**a**) Red laser light, (**b**) green laser light.

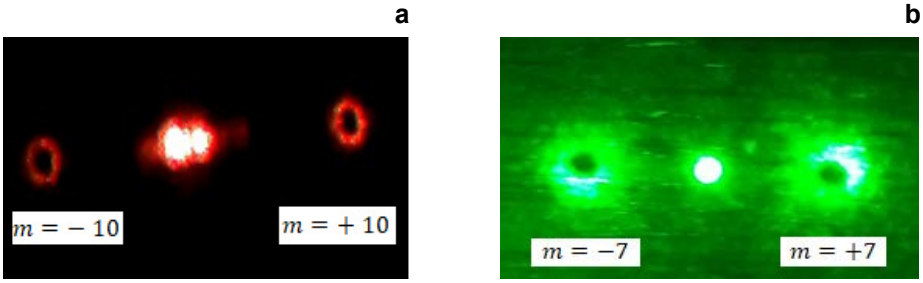

Fig. 12. Structured electromagnetic waves. (**a**) Red laser light, (**b**) green laser light.

at 500–570 nm is $m = \pm 7$ as shown in Fig. 12**b**. Topological load value $m = -7$ rotates clockwise while $m = +7$ rotates counterclockwise. The reason the green light is brighter in the image is due to its higher output intensity of the illuminator used. In addition, the reason the light spreads to the plane in Fig. 12**b** may be due to the feature of the illuminator used.

In Fig. 13, hologram masks with topological values are shown for $m = 10$, $m = 1$, $m = -1$, $m = -10$ and structured electromagnetic waves corresponding to these hologram masks, respectively. The distance between the images of the structured electromagnetic waves obtained and the SLM (between CCD and SLM) is approximately 1.5 meters. As seen in the figures, as the topological load value (m) increases, the distance between the dark spot and the bright ring (radius of the bright ring) also increases.

In Figure 14, the structured EMWs obtained by BIGMAN [45] with LCD-based SLM and the structured EMWs obtained by using DLP-based SLM are visually compared. As seen in the figure, the same twisted lights can be seen in both pictures according

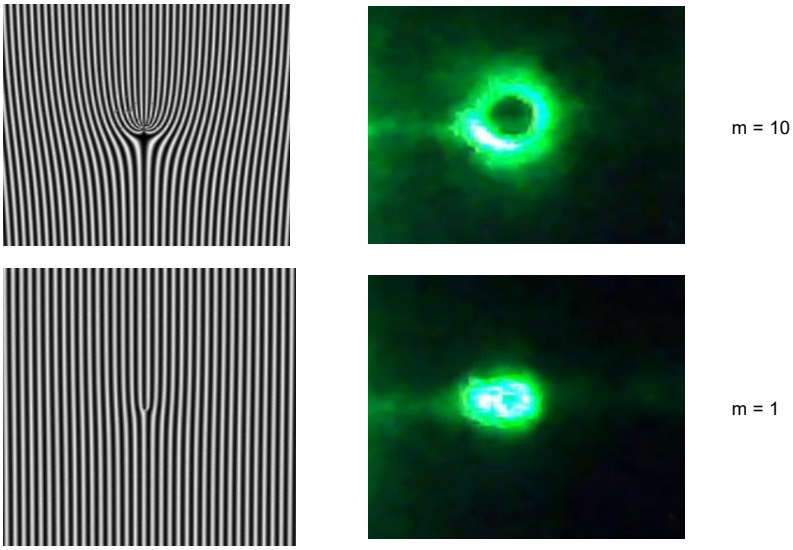

Fig. 13. Hologram and structured electromagnetic waves with a topological load.

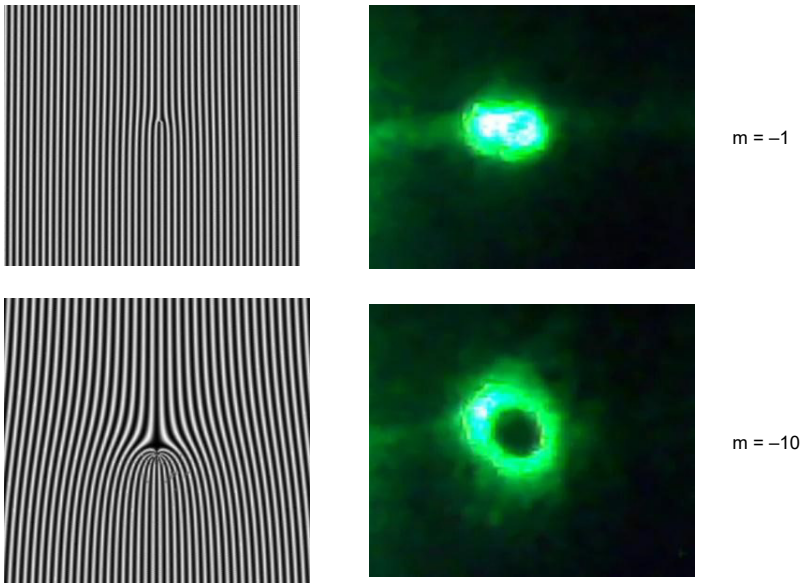

Fig. 13. Continued.

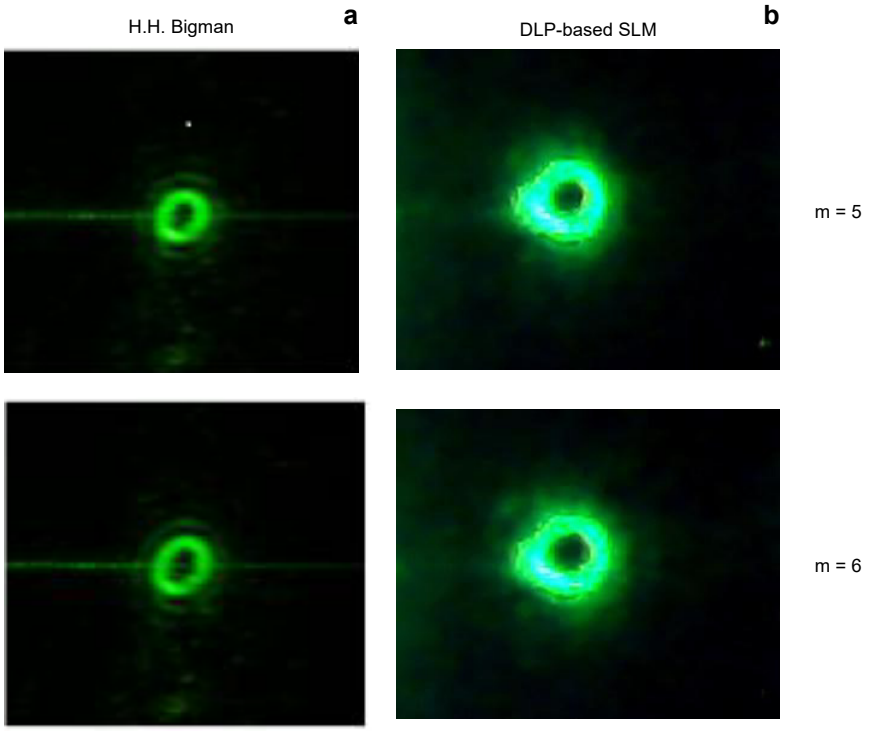

Fig. 14. (**a**) Structured electromagnetic waves obtained by Bigman H.H in his Master's work. (**b**) Structured electromagnetic waves that we obtained with the SLM we designed.

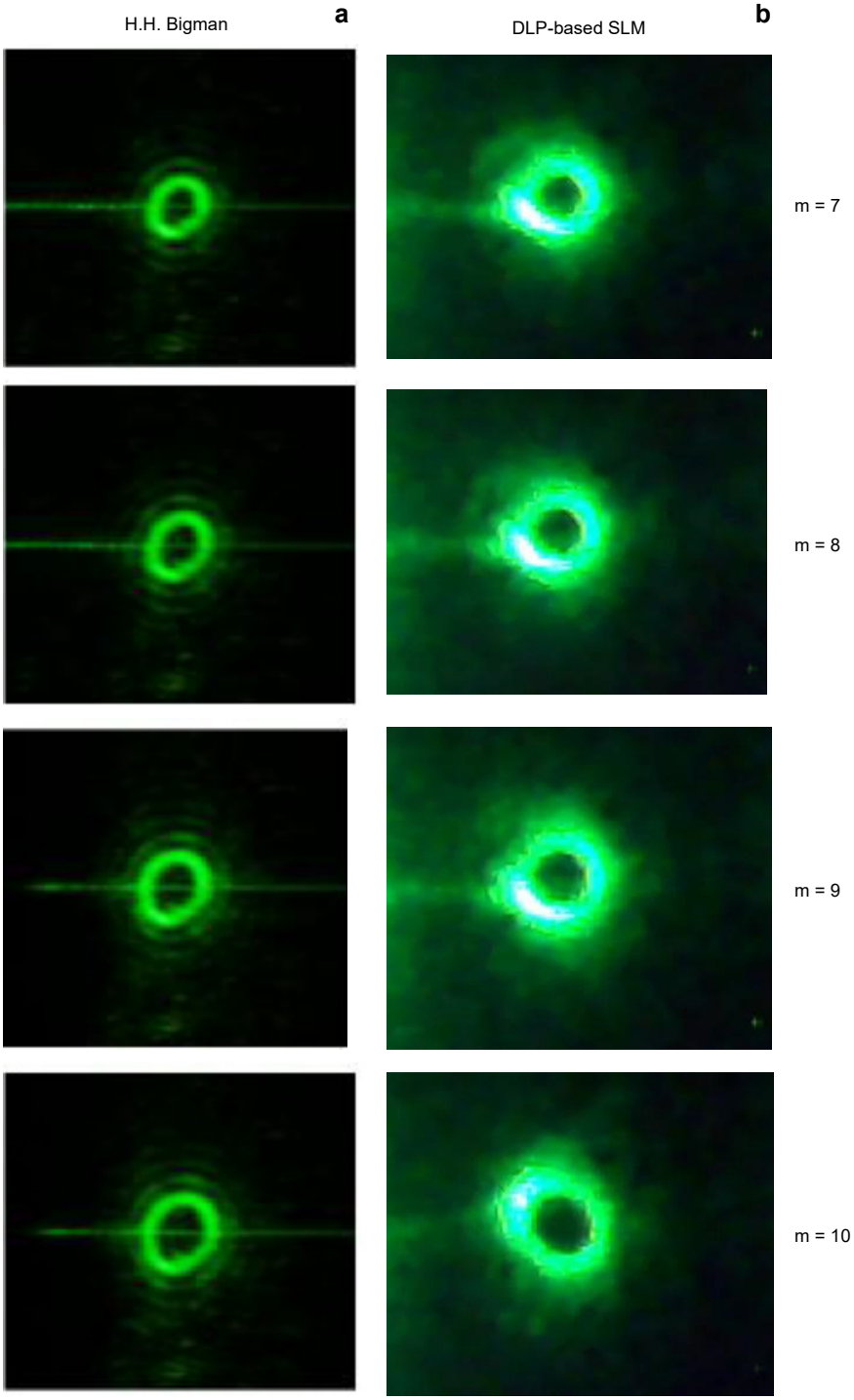

Fig. 14. Continued.

to the topological values. However, the twisted lights we have obtained are seen with a brighter reflection due to light intensity. As a result, a visual comparison of the structured electromagnetic waves we obtained and the structured electromagnetic waves obtained with a commercial SLM is shown in Fig. 14.

6. Conclusion

SLMs are versatile tools for optical teaching and scientific researches. They can be used in phase shaping, holography, and optical control fields. SLMs can be used as a useful tool in both industrial areas and undergraduate and graduate electric laboratories. However, their use in these areas is limited due to their high cost. By carrying out this study, we have demonstrated that SLMs can be produced at lower cost and they can be used more widely, both for industrial and scientific purposes. Therefore, it has been shown in our study that a low-cost SLM can be created by modification of a DLP-based projector, and that these devices can be alternatives to existing expensive SLMs. The SLM we designed can also be used in holography and in structuring electromagnetic waves. At the same time, in addition to cost, it has been observed that SLM designed may be more advantageous than a commercial SLM in terms of resolution, reflection rate and reaction speed. DLP-based SLMs can be developed for use in structuring EMWs in the UV region.

References

[1] Brüning R., Ndagano B., McLaren M., Schröter S., Kobelke J., Duparré M., Forbes A., *Data transmission with twisted light through a free-space to fiber optical communication link*, Journal of Optics **18**(3), 2016, article ID 03LT01, DOI: 10.1088/2040-8978/18/3/03LT01.

[2] Weiner A.M., *Femtosecond pulse shaping using spatial light modulators*, Review of Scientific Instruments **71**(5), 2000, pp. 1929–1960, DOI: 10.1063/1.1150614.

[3] Jayasinghe A.K., Rohner J., Hutson M.S., *Holographic UV laser microsurgery*, Biomedical Optics Express **2**(9), 2011, 2590–2599, DOI: 10.1364/BOE.2.002590.

[4] Hornbeck I.L.J., Alstyne V., Nelson W.E., *Spatial light modulator and method*, U.S. Patent No.5,096,279, 1992.

[5] Torres J.P., *Multiplexing twisted light*, Nature Photonics **6**(7), 2012, pp. 420–422, DOI: 10.1038/nphoton.2012.154.

[6] Nayar S.K., Branzoi V., Boult T.E., *Programmable imaging using a digital micromirror array*, [In] *Proceedings of the 2004 IEEE Computer Society Conference on Computer Vision and Pattern Recognition, 2004. CVPR 2004*, 2004, pp. I-I, DOI: 10.1109/CVPR.2004.1315065.

[7] Huang D., Timmers H., Roberts A., Shivaram N., Sandhu A.S., *A low-cost spatial light modulator for use in undergraduate and graduate optics labs*, American Journal of Physics **80**(3), 2012, pp. 211–215, DOI: 10.1119/1.3666834.

[8] Dudley D., Duncan W.M., Slaughter J., *Emerging digital micromirror device* (*DMD*) *applications*, Proc. SPIE **4985**, MOEMS Display and Imaging Systems, (20 January 2003), pp. 14–25, DOI: 10.1117/12.480761.

[9] Jing H., Cheng W., Zhang W., Lyu R., *OAM based wireless communications with non-coaxial UCA transceiver*, [In] *2019 IEEE 30th Annual International Symposium on Personal, Indoor and Mobile Radio Communications* (*PIMRC*), 2019, pp. 1–6, DOI: 10.1109/PIMRC.2019.8904219.

[10] FENG P.-Y., QU S.-W., YANG S., *OAM-generating transmitarray antenna with circular phased array antenna feed*, IEEE Transactions on Antennas and Propagation **68**(6), 2020, pp. 4540–4548, DOI: 10.1109/TAP.2020.2972393.
[11] JING H., CHENG W., LI Z., ZHANG H., *Concentric UCAs based low-order OAM for high capacity in radio vortex wireless communications*, Journal of Communications and Information Networks **3**(4), 2018, pp. 85–100, DOI: 10.1007/s41650-018-0036-z.
[12] PARK M.-C., LEE B.-R., SON J.-Y., CHERNYSHOV O., *Properties of DMDs for holographic displays*, Journal of Modern Optics **62**(19), 2015, pp. 1600–1607, DOI: 10.1080/09500340.2015.1054445.
[13] TAKAKI Y., OKADA N., *Hologram generation by horizontal scanning of a high-speed spatial light modulator*, Applied Optics **48**(17), 2009, pp. 3255–3260, DOI: 10.1364/AO.48.003255.
[14] NESBITT R.S., SMITH S.L., MOLNAR R.A., BENTON S.A., *Holographic recording using a digital micromirror device*, Proc. SPIE **3637**, Practical Holography XIII, (25 March 1999), pp. 12–20, DOI: 10.1117/12.343767.
[15] SUN B., EDGAR M. P., BOWMAN R., VITTERT L.E., WELSH S., BOWMAN A., PADGETT M.J., *3D computational imaging with single-pixel detectors*, Science **340**(6134), 2013, pp. 844–847, DOI: 10.1126/science.1234454.
[16] ZHU P., FAJARDO O., SHUM J., YAN-PING ZHANG SCHÄRER, FRIEDRICH R.W., *High-resolution optical control of spatiotemporal neuronal activity patterns in zebrafish using a digital micromirror device*, Nature Protocols **7**(7), 2012, pp. 1410–1425, DOI: 10.1038/nprot.2012.072.
[17] REN Y.-X., LI M., HUANG K., WU J.-G., GAO H.-F., WANG Z.-Q., LI Y.-M., *Experimental generation of Laguerre–Gaussian beam using digital micromirror device*, Applied Optics **49**(10), 2010, pp. 1838–1844, DOI: 10.1364/AO.49.001838.
[18] RODRIGO P. J., PERCH-NIELSEN I.R., GLÜCKSTAD J., *High-speed phase modulation using the RPC method with a digital micromirror-array device*, Optics Express **14**(12), 2006, pp. 5588–5593, DOI: 10.1364/OE.14.005588.
[19] YU, C., LI, J., LI, X., REN, X., GUPTA B.B., *Four-image encryption scheme based on quaternion Fresnel transform, chaos and computer generated hologram*, Multimedia Tools and Applications **77**(4), 2018, pp. 4585–4608, DOI: 10.1007/s11042-017-4637-6.
[20] SCHWERDTNER A., *Method of computing a hologram for reconstructing an object using a display device*, US Patent No: 10,884,377, 2021.
[21] LEISTER N., HAUSSLER R., SCHWERDTNER A., *Method and a display device for generating a holographic reconstruction of an object*, US Patent No: 10,401,794, 2019.
[22] DALLAS W.J., *Phase quantization in holograms—A few illustrations*, Applied Optics **10**(3), 1971, pp. 674–676, DOI: 10.1364/AO.10.000674.
[23] GOODMAN J.W., SILVESTRI A.M., *Some effects of Fourier-domain phase quantization*, IBM Journal of Research and Development **14**(5), 1970, pp. 478–484, DOI: 10.1147/rd.145.0478.
[24] NAIDU P.S., *Quantization noise in binary holograms*, Optics Communications **15**(3), 1975, pp. 361–365, DOI: 10.1016/0030-4018(75)90246-1.
[25] BROWN B.R., LOHMANN A.W., *Computer-generated binary holograms*, IBM Journal of Research and Development **13**(2), 1969, pp. 160–168, DOI: 10.1147/rd.132.0160.
[26] TRIPATHY A.K., DAS S.K., SUNDARAY M., TRIPATHY S.K., *Particle swarm optimization for the design of high diffraction efficient holographic grating*, American Journal of Computer Science and Engineering Survey **3**(1), 2015, pp. 28–33.
[27] TRIPATHY A.K., TRIPATHY S.K., PATTANAIK S.R., DAS S.K., *A new algorithm for reconstruction of a computer-generated hologram* (*CGH*), The Computer Journal **64**(2), 2021, pp. 245–253, DOI: 10.1093/comjnl/bxaa151.
[28] LOHMANN A.W., PARIS D.P., *Binary Fraunhofer holograms, generated by computer*, Applied Optics **6**(10), 1967, pp. 1739–1748, DOI: 10.1364/AO.6.001739.
[29] POON T.C., LIU J.P., *Introduction to Modern Digital Holography with MATLAB*, Cambridge University Press, 2014.

[30] Product Folder Order Now DLP7000 DLP7000 DLP ® 0.7 XGA 2x LVDS Type A DMD, 2012. www.ti.com (accessed February 5, 2021).
[31] Douglass M.R., *Lifetime estimates and unique failure mechanisms of the digital micromirror device* (*DMD*), [In] *1998 IEEE International Reliability Physics Symposium Proceedings. 36th Annual* (*Cat. No. 98CH36173*), 1998, pp. 9–16, DOI: 10.1109/RELPHY.1998.670436.
[32] LCOS-SLM (Liquid Crystal on Silicon-Spatial Light Modulator), www.hamamatsu.com (accessed July 24, 2020).
[33] Dlp9000Xuv, 2019. www.ti.com (accessed July 24, 2020).
[34] https://www.ti.com/product/DLP5500 (accessed October 30, 2021).
[35] *Application Note How to connect the Control board Interface* (*UART, Communication and Synchronization*), 2010, pp. 1–10. http://monitor.espec.ws/files/5-pin-interface_-version-2.9_-01.02.2010_194.pdf (accessed August 26, 2021).
[36] Cox M.A, Drozdov A.V., *Converting a Texas Instruments DLP4710 DLP evaluation module into a spatial light modulator*, Applied Optics **60**(2), 2021, pp. 465–469, DOI: 10.1364/AO.412729.
[37] Panarin S., Müller J., Prabhakar S., Fickler R., *Spatial structuring of light for undergraduate laboratories*, American Journal of Physics **89**(2), 2021, pp. 210–219, DOI: 10.1119/10.0002365.
[38] Carpentier A.V., Michinel H., Salgueiro J.R., et al., *Making optical vortices with computer-generated holograms*, American Journal of Physics **76**(10), 2008, pp. 916–921, DOI: 10.1119/1.2955792.
[39] Brambilla M., Battipede F., Lugiato L.A., Penna V., Prati F., Tamm C., Weiss C.O., *Transverse laser patterns. I. Phase singularity crystals*, Physical Review A **43**(9), 1991, p. 5090, DOI: 10.1103/PhysRevA.43.5090.
[40] Beijersbergen M.W, Allen L., Van der Veen H.E.L.O., Woerdman J.P., *Astigmatic laser mode converters and transfer of orbital angular momentum*, Optics Communications **96**(1–3), 1993, pp. 123–132, DOI: 10.1016/0030-4018(93)90535-D.
[41] Slinger C., Cameron C., Stanley M., *Computer-generated holography as a generic display technology*, Computer **38**(8), 2005, pp. 46–53, DOI: 10.1109/MC.2005.260.
[42] Heckenberg N.R., McDuff R., Smith C.P., White A.G., *Generation of optical phase singularities by computer-generated holograms*, Optics Letters **17**(3), 1992, pp. 221–223, DOI: 10.1364/OL.17.000221.
[43] Trester S., *Computer simulated holography and computer generated holograms*, American Journal of Physics **64**(4), 1996, pp. 472–478, DOI: 10.1119/1.18194.
[44] Nathan A.J., Scobell A., *Stereolithography Materials, Processes and Applications*, Springer Science & Business Media, New York, 2011.
[45] Bigman H.H., *Zero Spatial Chirp Vortices from Supercontinuum Modulation*, San Diego State University, 2012.

Received August 26, 2021
in revised form November 4, 2021